Electromagnetic Decay of the Σ^{*0} to $\Lambda\gamma$

D. Keller[1] and K. Hicks[1]
(The CLAS Collaboration)
[1] *Ohio University, Department of Physics, Athens, OH 45701, USA*
(Dated: October 8, 2010)

The electromagnetic decay $\Sigma^0(1385) \to \Lambda\gamma$ was studied using the CLAS detector at the Thomas Jefferson National Accelerator Facility. A real photon beam with a maximum energy of 3.8 GeV was incident on a proton target, producing an exclusive final state of $K^+\Sigma^{*0}$. We report the ratio of decay widths $\Sigma^0(1385) \to \Lambda\gamma/\ \Sigma^0(1385) \to \Lambda\pi^0 = 1.42 \pm 0.12\%$ where the uncertainty includes statistical and systematic uncertainties. This result is slightly smaller, but consistent within uncertainties, than a previous measurement by Taylor *et al.*. This ratio is about 2-3 times larger than most theoretical predictions.

PACS numbers:

INTRODUCTION

One well-known success of the constituent quark model (CQM) is its prediction of the magnetic moments of the low-mass baryons, using just the SU(6) wave functions [1, 2]. Calculations for the magnetic moments [3], assuming that quarks behave as pointlike Dirac dipoles, is typically within ∼10% of the current measured values [4]. However, today we know that the spin of the proton is much more complex, with only about one-third of the proton's spin coming from the valence quarks [5] and the rest of the spin from a combination of the gluon spins and orbital motion of the quarks [6, 7]. Clearly, the CQM is an over-simplification of the spin dynamics inside baryons yet somehow the CQM captures the degrees of freedom that are relevant to the magnetic moments that have been measured. Further measurements of baryon magnetic moments, via electromagnetic decay of excited baryons, will continue to test our understanding of baryon wavefunctions.

Experimentally, it is difficult to measure the EM transitions of decuplet-to-octet baryons because of competition between electromagnetic (EM) decays and strong decays. For example, the branching ratio for EM decay of the Δ resonance has been measured at about 0.55% [4] and branching ratios for other decuplet baryons are predicted to be of the same order of magnitude. For the Δ, it is possible to measure the EM transition form factors directly via pion photoproduction [8, 9].

It has been shown [10] that pion cloud effects contribute significantly (∼40%) to the $\gamma p \to \Delta^+$ magnetic dipole transition form factor, $G_M(Q^2)$, at low Q^2 (below ~ 0.1 GeV^2). In the naive non-relativistic quark model [12], the value of $G_M(0)$ is directly proportional to the proton magnetic moment [10], and measurements of G_M near $Q^2 = 0$ can only be explained (within this quark model) if the experimental magnetic moment is lowered by about 30%. This again suggests that the CQM is an over-simplification of reality.

To extend these measurements to the other decuplet baryons, which have non-zero strangeness, hyperons must be produced through strangeness-conserving reactions. Then their EM decay, which has a small branching ratio, must be measured directly. Although these measurements are difficult, it is important to measure the EM decays of strange baryons because we get information on their wavefunctions, which in turn constrains theoretical models of baryon structure.

The measurements of EM transition form factors for decuplet baryons with strangeness may also be sensitive to meson cloud effects, at roughly the same level. Comparison of data for the EM decay of decuplet hyperons, Σ^*, to the predictions of quark models provides a measure of the importance of meson cloud diagrams in the $\Sigma^* \to Y\gamma$ transition.

Here, we present measurements of the EM decay $\Sigma^{*0} \to \Lambda\gamma$ normalized to the strong decay $\Sigma^{*0} \to \Lambda\pi^0$. The present results can be compared to previous measurements of the Σ^{*0} EM decay [11] that had a larger uncertainty (∼25% statistical and ∼15% systematic uncertainty). The smaller uncertainties here are due to a larger data set (more than 10 times bigger) and subsequently a better control over systematic uncertainties. The reduced uncertainty is important because, as mentioned above, meson cloud effects are predicted to be on the order of ∼30-40%. In order to know quantitatively the effect of meson clouds for baryons with non-zero strangeness, it is desirable to keep measurement uncertainties below ∼10%.

There are many theoretical calculations of the EM decays of decuplet hyperons such as: the non-relativistic quark model (NRQM) [13, 14], a relativized constituent quark model (RCQM) [15], a chiral constituent quark model (χCQM) [16], the MIT bag model [17], the bound-state soliton model [18], a three-flavor generalization of the Skyrme model that uses the collective approach [19, 20], an algebraic model of hadron structure [21], and heavy baryon chiral perturbation theory (HBχPT) [22], among others. Table I summarizes the theoretical pre-

TABLE I: Theoretical predictions for the models shown and experimental values for the electromagnetic decay widths (in keV).

Model	$\Delta(1232) \to N\gamma$	$\Sigma(1193) \to \Lambda\gamma$	$\Sigma(1385) \to \Lambda\gamma$
NRQM [13, 14, 17]	360	8.6	273
RCQM [15]		4.1	267
χCQM [16]	350		265
MIT Bag [17]		4.6	152
Soliton [18]			243
Skyrme [19, 20]	309-326		157-209
Algebraic model [21]	341.5	8.6	221.3
HBχPT [22]†	(670-790)		290-470
Experiment[4]	660±47	9.1±0.9	470±160

† Normalized to experiment for the $\Delta \to N\gamma$ range shown.

dictions and experimental branching ratios for the EM transitions of interest.

A comprehensive study of electromagnetic strangeness production has been undertaken using the CLAS detector at the Thomas Jefferson National Accelerator Facility. Many data on ground-state hyperon photoproduction have already been published [23–25] using data from the so-called $g1$ and $g11$ data sets. The $g1$ experiment had an open trigger [23] and lower data acquisition speed, whereas the $g11$ experiment required at least two particles to be detected [25], and higher beam current, giving a much higher data acquisition speed. The result is that the $g11$ data had over 20 times more useful triggers than in the $g1$ data. The present results used the $g11$ data set, whereas Taylor *et al.* used the $g1$ data set. Previous CLAS results give a great deal of confidence to the corresponding calibration of these data sets [25].

The EM decay of the Σ^{*0} is only about 1% of the total decay width. To isolate this signal from the dominant strong decay $\Sigma^{*0} \to \Lambda\pi^0$, the missing mass of the detected particles, $\gamma p \to K^+\Lambda(X)$ is calculated. Because of its proximity to the π^0 peak in the mass spectrum from strong decay, the EM decay signal is difficult to separate using simple peak-fitting methods. The strategy here is to understand and eliminate as much background as possible using standard kinematic cuts, and then use a kinematic fitting procedure for each channel. As described below, by varying the cut points on the confidence levels of each kinematic fit, the systematic uncertainty associated with the extracted ratio for EM decay can be quantitatively determined. The increased statistics for the $g11$ data helps greatly to study the systematic uncertainty.

THE EXPERIMENT

For the present measurements, a bremsstrahlung photon beam was produced from a 4.019 GeV electron beam, resulting in a photon energy range of 1.6-3.8 GeV. The photon energy was deduced from a magnetic spectrometer [26] that "tagged" the electron with an energy resolution of $\sim 2\%$. A liquid-hydrogen target was used that was 40 cm long and placed such that the center of the target sat at 10 cm upstream from the center of CLAS. As mentioned above, a two particle trigger in coincidence with the tagged electron was used. The data acquisition recorded approximately 20 billion events. Details of the experimental setup are given elsewhere [25, 27].

Event Selection

We selected events for the reaction $\gamma p \to K^+\Sigma^{*0}$, where the Σ^{*0} decays with 87.0±1.5% probability to $\Lambda\pi^0$ and 1.3±0.4% probability to $\Lambda\gamma$ [4]. The Λ then decays with 63.9±0.5% probability to $p\pi^-$, leading to the final states $\gamma p \to K^+p\pi^-\pi^0$ and $\gamma p \to K^+p\pi^-\gamma$, respectively [4]. The charged particles are detected by the CLAS drift chambers, giving their momentum, and by the time-of-flight scintillators, giving their velocity. The π^0 and γ must be deduced indirectly using conservation of energy and momentum.

In the present analysis, the mass of the detected particles were calculated from the measured velocity and momentum. The mass is given by

$$m_{cal} = \sqrt{\frac{p^2(1-\beta^2)}{\beta^2 c^2}}, \qquad (1)$$

where $\beta = L/ct_{meas}$ for path length L and measured time of flight t_{meas}, and c is the speed of light. The pions, kaons, and protons were identified using mass cuts of $0.0 \le M_{\pi^-} \le 0.3$ GeV, $0.3 < M_{K^+} < 0.8$ GeV, and $0.8 \le M_p \le 1.2$ GeV, respectively. From this initial identification it is possible to incorporate additional timing information to improve event selection with quality constraints. The time of flight t_{meas} is the time difference between the event vertex time and the time at

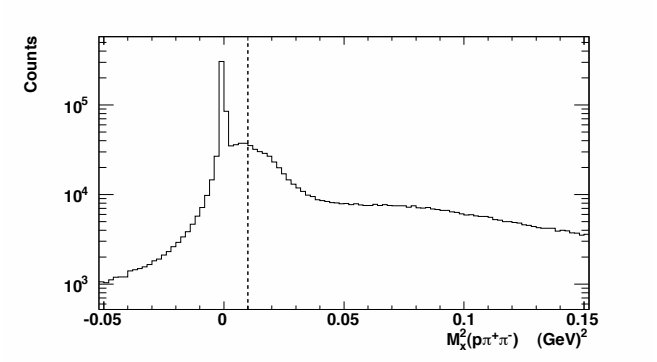

FIG. 1: Missing mass squared (M_x^2) for the reaction $\gamma p \to p\pi^+\pi^-(X)$ where the π^+ was a potentially misidentified kaon. The dotted line indicates the cut used.

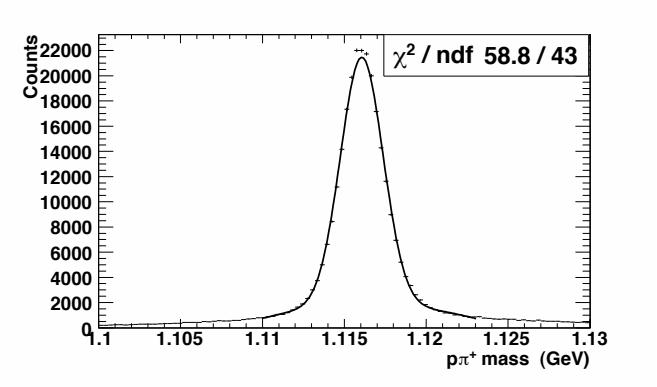

FIG. 2: The invariant mass of the p-π^- showing the Λ peak with a Gaussian fit giving a $\sigma = 1.3$ MeV.

which the particle strikes the time-of-flight scintillator walls on the outside shell of the CLAS detector. We define $\Delta t = t_{meas} - t_{cal}$, where t_{cal} is the time of flight calculated for an assumed mass such that

$$t_{cal} = \frac{L}{c}\sqrt{1 + \left(\frac{m}{p}\right)^2}, \qquad (2)$$

where m is the assumed mass for the particle of interest and p is the momentum magnitude. A cut on Δt or m_{cal} should be effectively equivalent.

Using Δt for each particle it is possible to reject events that are not associated with the correct RF beam bunches, which are separated by 2 ns. This is done by accepting only events with $|\Delta t| \leq 1$ ns.

Energy loss for charged particles as they pass through various materials in the CLAS detector requires an adjustment to the particle energy. The charged particle's momentum is corrected for the average dE/dx losses in the target material, target wall, carbon epoxy pipe, and the start counter scintillators surrounding the target. After correcting for energy loss, several kinematic cuts are applied as described below.

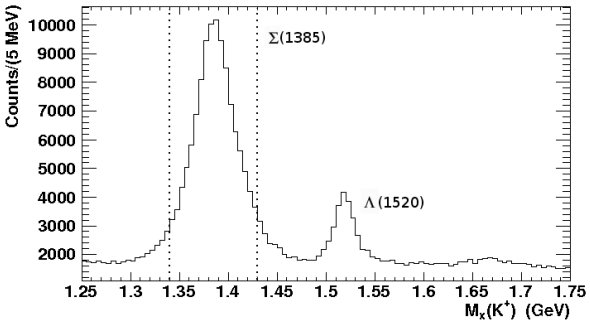

FIG. 3: Missing mass for the reaction $\gamma p \to K^+(X)$, for events passing the cut on the Λ mass.

Due to the finite resolution of the measured velocity and momentum, in addition to particle decay-in-flight, it is possible that some kaons could be misidentified as pions. To clean up the kaon signal for the analysis, it is common to purposely recalculate the energy of the identified kaon using the mass of the pion. Then the missing mass squared is studied for the reaction $\gamma p \to p\pi^+\pi^-(X)$, where the π^+ is actually identified by the above mass cuts as a K^+. A spike at zero mass squared indicates that the reaction $\gamma p \to p\pi^+\pi^-$ is prominent. The particle misidentified events can be removed by cutting slightly above zero, as shown in Fig. 1. A cut at 0.01 GeV^2, shown as the dotted line in the Figure, is used so as to not cut into the good K^+ events. Reactions such as $\rho \to \pi^+\pi^-$, where the π^+ is mistakenly identified as a K^+, are also eliminated by this cut.

The four-momentum of the detected Λ was reconstructed from the proton and π^- four-momenta (see Fig. 2). The invariant mass peak was fitted with a Gaussian to achieve a resolution of $\sigma = 1.3$ MeV, which is consistent with the instrumental resolution. After cutting on the Λ in the range 1.112 to 1.119 GeV, the excited-state hyperon mass spectrum (constructed from the missing mass off the K^+) is shown in Fig. 3.

After making a cut on the Σ^* peak from 1.34-1.43, as shown in Fig. 3, one can study the missing mass off of the Λ, shown in Fig. 4. Small peaks are seen at the mass of the kaon and also at the $K^*(892)$ mass. The kaon peak is from exclusive $\gamma p \to K^+\Lambda$ production due to accidental coincidences, which can easily be cut out. The dotted line shows the $M_x(\Lambda) > 0.55$ GeV cut used to eliminate this background.

After the foregoing cuts, the missing mass of the reaction $\gamma p \to K^+ p\pi^-(X)$ is shown in Fig. 5. A very prominent peak is seen at the mass of the π^0 with a very small number of counts at zero missing mass due to the EM decay. The counts above the π^0 peak are mostly due to the $\gamma p \to K^+\Sigma^0(X)$ reaction from photoproduction of higher mass hyperons. Because the tail of the π^0 peak continues over into the zero missing mass region, it is dif-

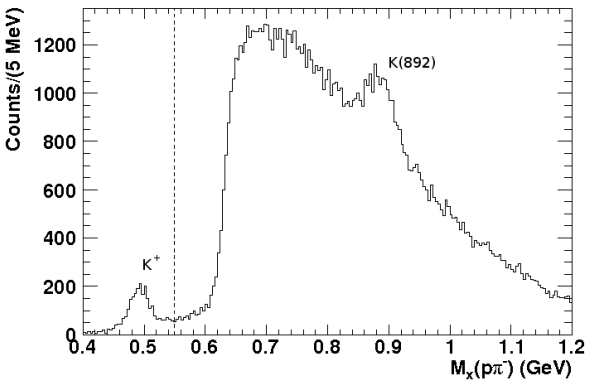

FIG. 4: Missing mass for the reaction $\gamma p \to \Lambda(X)$ for events passing cuts on the Λ and Σ^* masses.

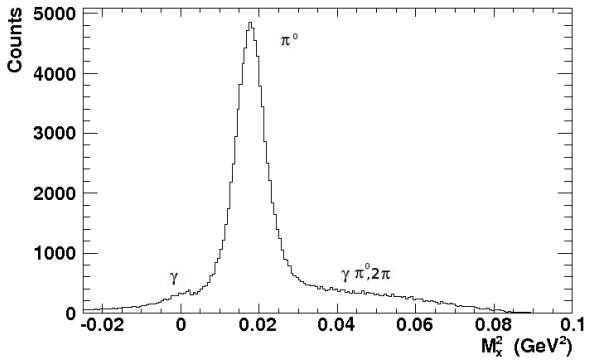

FIG. 5: Missing mass squared for the reaction $\gamma p \to K^+ p\pi^-(X)$ after all kinematic cuts.

ficult to cleanly resolve the EM decay signal. A standard Gaussian fit cannot easily separate the EM decay from the various backgrounds, so care must be take to use a method that can take the π^0 leakage into account.

KINEMATIC FITTING

The kinematic fitting technique takes advantage of the information in the measured kinematic variables and their uncertainties to fit constraints of energy and momentum conservation, thereby improving the measured quantities through use of constraint equations. This procedure is useful to improve the separation of signal from background. The method of Lagrange multipliers is the approach implemented here to fit the constraints with a least squares criteria [28].

Assume there are n independently measured data values y, which in turn are functions of m unknown variables q_i, with $m \leq n$. The condition that $y = f_k(q_i)$ is introduced where f_k is a function dependent on the data points that are being tested for each k independent variable at each point.

Because each y_k is a measurement with corresponding standard deviation σ_k, the equation $y_k = f_k(q_i)$ cannot be satisfied exactly for $m < n$. It is possible to require that the relationship be closely numerically satisfied by defining the χ^2 relation such that

$$\chi^2 = \sum_k \frac{(y_k - f_k(q))^2}{\sigma_k^2},$$

and demanding that selected values of q_i preserve only the smallest χ^2.

The unknowns are divided into a set of measured variables ($\vec{\eta}$) such as the measured momentum components and unmeasured variables ($\vec{u}$) such as missing momentum. Now introduce a variable $\mathcal{L}_i$ to be used for each constraint equation. These variables are the Lagrange multipliers and are used to write the equation for χ^2 for a set of constraint equations $\mathcal{F}$ such that,

$$\chi^2(\vec{\eta}, \vec{u}, \mathcal{L}) = (\vec{\eta}_0 - \vec{\eta})^T V^{-1} (\vec{\eta}_0 - \vec{\eta}) + 2\mathcal{L}^T \mathcal{F} \quad (3)$$

where $\vec{\eta}_0$ is a vector of initial measured quantities and V^{-1} is the inverse of the covariance matrix containing all of the known uncertainties on the measured parameters. The χ^2 minimization occurs by differentiating χ^2 with respect to each of the variables, while linearizing the constraint equations and obtaining improved measured values from the fit. The output for of the improved measured values are used as the input for a series of iterations. The iteration procedure is continued until the difference in magnitude between the current χ^2 and the previous value is smaller than $\Delta\chi^2_{test}$ ($\leq$0.001).

The implemented covariance matrix V was corrected for multiple scattering and the energy loss in the target cell, the carbon epoxy scattering chamber, and the start counter. These corrections to the diagonal terms in the covariance matrix are applied according to the distance each charged particle travels through the corresponding material.

SIMULATIONS

A Monte Carlo simulation of the CLAS detector was performed using GEANT [29], set up for the $g11$ run conditions. Events were generated for the radiative channels ($\Sigma^0(1385) \to \Lambda\gamma$), the normalization reaction ($\Sigma^0(1385) \to \Lambda\pi^0$), and several background reactions, see Table II for a complete list. Using the data as a guide, the photon beam energy dependence of K^+ production and the K^+ angular dependence were used iteratively to tune the Monte Carlo to match the data. After reconstruction, the kinematic distributions for the proton, π^-, and K^+ agreed very well between the Monte Carlo and

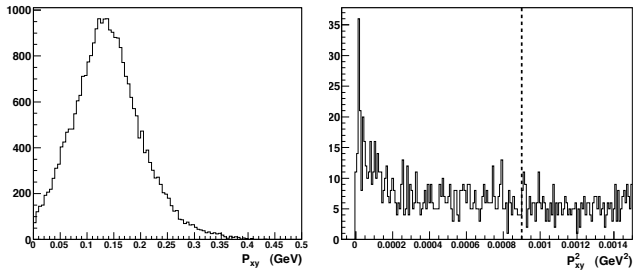

FIG. 6: Transverse missing momentum (left) and transverse missing momentum squared (right)for the reaction $\gamma p \rightarrow K^+\Lambda(X)$

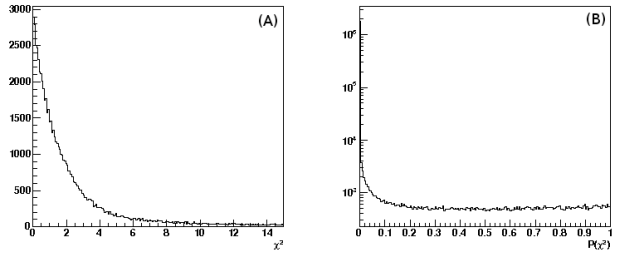

FIG. 7: (A) χ^2 distribution and (B) Confidence Level distribution, for a missing π^0 hypothesis in the kinematic fit.

the data. The generated Monte Carlo events were analyzed using the same analysis procedure as for the data.

After studying the various channels of interest and background, a t-dependence of 2.0 GeV^2 was used for the generated $\gamma p \rightarrow K^+\Lambda(1405)$ channel. The differential cross section from data were used for the generator to produce all the Σ^* simulations.

ANALYSIS PROCEDURE

Because of the possibility of a false EM decay signal caused by double bremsstrahlung in the radiator, care is taken to minimize this effect. The reaction $\gamma_1 + \gamma_2 p \rightarrow K^+\Lambda + \gamma_1$ can mimic the final state of interest $\gamma p \rightarrow K^+\Lambda\gamma$. The γ_1 from double bremsstrahlung will point down the z-axis (along the beam), which can also occur if the event is accidental or due to inefficiencies in the tagger plane from incorrect electron selection. By calculating the transverse missing momentum ($P^2_{xy} = P^2_x + P^2_y$) it is possible to eliminate double bremsstrahlung. The peak at small values in the distribution in Fig. 6 was removed with the dashed line cut at $P_{xy} > 0.03$ GeV/c.

To ensure only high quality Λ events, a kinematic fit can be used on the proton and π^- track to a Λ invariant mass hypothesis. To ensure that no systematic bias is introduced, we fit the Λ invariant mass together with a total missing mass hypothesis. Each track for all detected particles is fit to a particular missing particle hypothesis, while requiring that the proton and π^- be constrained to have an invariant mass of the Λ. This is done by using the undetected particle mass in the constraint equation while also meeting the Λ constraint. After the detected particle tracks are kinematically fit, each event is filtered with a confidence level cut. In this fit there are three unknowns ($\vec{p}_x$) and five constraint equations, four from conservation of momentum and the additional invariant mass condition. This makes it a 2C kinematic fit.

To separate the various contributions of the Σ^{*0} EM decay and the strong decay ($\Lambda\pi^0$), the events were fit using the hypotheses for each topology:

$$\gamma p \rightarrow K^+ p\pi^-(\pi^0) \;\; \text{2C}$$
$$\gamma p \rightarrow K^+ p\pi^-(\gamma) \;\; \text{2C}.$$

The constraint equations are

$$\mathcal{F} = \begin{bmatrix} (E_\pi + E_p)^2 - (\vec{p}_\pi + \vec{p}_p)^2 - M^2_\Lambda \\ E_{beam} + M_p - E_K - E_p - E_\pi - E_x \\ \vec{p}_{beam} - \vec{p}_K - \vec{p}_p - \vec{p}_\pi - \vec{p}_x \end{bmatrix} = \vec{0}, \quad (4)$$

where $\vec{P}_x$ and E_x are the momentum and energy of the undetected π^0 or γ.

To test the functionality of the kinematic fit used to separate the radiative signal from the overwhelming π^0 background, the probability density function for two degrees of freedom is used to fit the resulting χ^2 distribution. The fit function takes the form,

$$f(\chi^2) = \frac{P_0}{2} e^{-P_1\chi^2/2} + P_2, \quad (5)$$

where P_2 is a background term, P_1 is a quantitative closeness parameter (which gives a measure of how close the distribution in the histogram is to the ideal theoretical χ^2 distribution), and P_0 is for normalization. For a kinematic fit to a missing γ, with significant background contamination from the π^0, the χ^2 distribution will be highly distorted. The ideal P_1 from a fit to a χ^2 distribution with no background is determined from simulations. The deviation of the P_1 fit parameter from the ideal P_1 is used as an indicator of how much signal to background is going into the kinematic fit with the radiative hypothesis and how effective a confidence level cut is expected to be for that given deviation.

Using the π^0-hypothesis for the kinematic fit, the χ^2 distribution follows the trend of the probability density function for two degrees of freedom, see Fig 7A. The confidence level in Fig. 7B is flat and even for the vast majority of event.

For the γ-hypothesis, without any cuts to reduce the π^0 background, the χ^2 distribution does not conform to that expected for a 2C fit. Due to the sensitive nature of the χ^2 distribution for two degrees of freedom a fit to obtain the P_1 parameter does not return a realistic value.

This can be seen in the distorted shape of the distribution in Fig. 8A. Additionally, the confidence level distribution rises up near the low confidence end (Fig. 8B) and is clearly not as flat as the distribution in Fig. 7B. This is an indication that the vast majority of data being kinematically fit at this stage are not satisfying the base assumption of a massless missing particle. This suggests that, even with a high confidence level cut, there is still an overwhelming amount of π^0 events leaking through. However, it is possible to take an additional step in the kinematic fitting procedure for cleaner separation.

A two-step kinematic fitting procedure is used. First, a fit to a π^0-hypothesis is done and only the low confidence level ($P^a_\pi(\chi^2)$) events are retained, followed by a fit of these candidate events to a γ-hypothesis and retaining high confidence level ($P^b_\gamma(\chi^2)$) events. Because of the previous kinematic cuts, there should now be primarily π^0 background and the true EM decay signal. Any other background is expected to be very small relative to the signal and will be accounted for through simulations. By first fitting to a π^0-hypothesis and taking the low confidence level candidates, one reduces the probability that the surviving candidates will have a missing mass of the π^0 before they are fit to a γ-hypothesis.

The selection of the confidence level cuts $P^a_\pi(\chi^2)$, and $P^b_\gamma(\chi^2)$ is derived using simulations. After testing the ability to recover various mixed ratios, on the order of the expected experimental ratio ($\sim 1\%$), Monte Carlo (MC) was generated for a given ratio of the $\gamma p \to K^+\Sigma^{*0} \to K^+\Lambda\pi^0$ and $\gamma p \to K^+\Sigma^{*0} \to K^+\Lambda\gamma$ channels. The optimization occurs when considering both increase in statistical uncertainty from a higher $P^a_\pi(\chi^2)$ cut and the increase in MC ratio "recovery" uncertainty from a lower $P^a_\pi(\chi^2)$ cut. The final confidence level cut in $P^b_\gamma(\chi^2)$ is determined by the fit parameter P_1 indicating how much π^0 background is left after the $P^a_\pi(\chi^2)$ cut. Again statistical uncertainty and the MC ratio "recovery" uncertainty is considered in the optimization of the $P^b_\gamma(\chi^2)$ cut.

The results of the optimization study indicate that a confidence level cut of $P^a_\pi(\chi^2) < 0.1\%$ reduces the π^0 background well enough that a $P^b_\gamma(\chi^2) > 10\%$ cut can be used to isolate the radiative signal in the kinematic fit to γ.

After the two-step kinematic fitting procedure, one can again study the γ-hypothesis χ^2 fit now looks more like a standard distribution for two degree of freedom, see Fig. 8 (C). The confidence level now appears relatively flat in Fig. 8 (D), as it should. This is an indication that an improvement has been made on the quality of candidates going into the fit with respect to the hypothesis. This gives some assurance that the candidates going into the secondary fit can accurately be filtered with a confidence level cut.

To ensure the quality of the π^0 extraction, the same two-step kinematic fitting procedure is done by first fitting to a γ hypothesis and taking a low confidence level $P^a_\gamma(\chi^2)$ candidates, then fitting to the π^0 hypothesis and taking only the high confidence level $P^b_\pi(\chi^2)$ candidates.

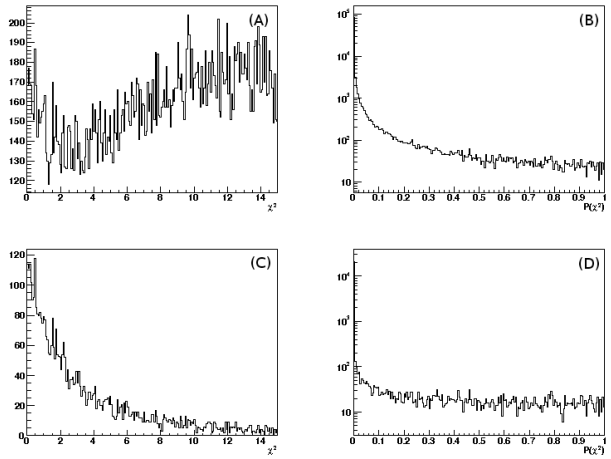

FIG. 8: (A) The χ^2 distribution and (B) the Confidence Level distribution for a missing γ hypothesis in the kinematic fit before the two-step kinematic fit. (C) The χ^2 distribution and the (D) the Confidence Level distribution for a missing γ hypothesis in the kinematic fit after the $P^a_\pi(\chi^2) < 0.1\%$ cut.

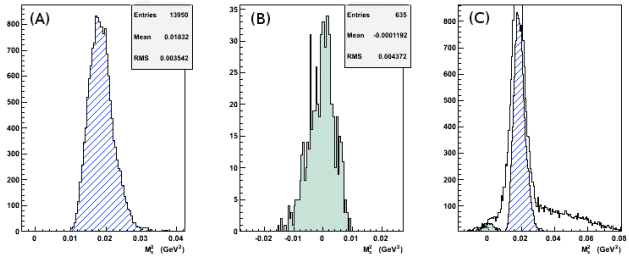

FIG. 9: (A) The n_π counts extracted using the confidence level cuts $P^a_\gamma < 0.01$ and $P^b_\pi > 0.1$. (B) The n_γ counts extracted using the confidence level cuts $P^a_\pi < 0.01$ and $P^b_\gamma > 0.1$. (C) The counts n_π and n_γ shown in the spectrum before any kinematic fit.

Once the confidence level cuts are optimized for extracting both the π^0 and radiative signal the final selected candidates in each cases can be seen in the missing mass spectrum, see Fig. 9. The extracted counts are shown for (A) the π^0,(B) the electromagnetic signal, and (C) together in the full spectrum of the missing mass squared.

The π^0 leakage into the γ channel is the dominant correction to the branching ratio. The final result also needs to be corrected for backgrounds, such as $K^* \to K^+X$ and decays to $\Sigma^+\pi^-$, as well as the contribution to the numerator from $\Lambda(1405) \to \Lambda\gamma$. Taking these backgrounds into consideration, and following the notation of Taylor

TABLE II: Acceptances (in units of 10^{-3}) for the channels used in the calculation of the branching ratios. Here there is a $P^a(\chi^2) < 0.1\%$ confidence level used with a $P^b(\chi^2) < 10\%$ cuts. The uncertainties are statistical only.

Reaction	A_π	A_γ	$A_{\gamma\pi}$
$\Lambda(1405) \to \Sigma^0\pi^0$	0.0495±0.0031	0.001±0.0001	1.189±0.019
$\Lambda(1405) \to \Sigma^+\pi^-$	0.029±0.002	0.0013±0.0001	0.0078±0.001
$\Lambda(1405) \to \Lambda\gamma$	0.0011±0.0001	1.65±0.031	0.0223±0.002
$\Lambda(1405) \to \Sigma^0\gamma$	0.170±0.012	0.191±0.009	0.437±0.013
$\Sigma(1385) \to \Lambda\pi$	1.421±0.0278	0.0321±0.002	0.0312±0.002
$\Sigma(1385) \to \Sigma^+\pi^-$	0.161±0.01	0.00254±0.001	0.00138±0.0006
$\Sigma(1385) \to \Lambda\gamma$	0.0184±0.002	2.335±0.039	0.0704±0.005
$\Sigma(1385) \to \Sigma^0\gamma$	0.191±0.011	0.058±0.0001	0.225±0.015
$\Lambda K^{*+} \to K^+\pi^0$	0.213±0.010	0.010±0.006	2.931±0.051
$\Lambda K^{*+} \to K^+\gamma$	0.0022±0.0001	0.158±0.003	2.351±0.046

et al. [11], the formula for the branching ratio is

$$\begin{aligned} R &= \frac{1}{\Delta n_\pi A_\gamma^\Sigma(\Lambda\gamma) - \Delta n_\gamma A_\pi^\Sigma(\Lambda\gamma)} \\ &\times \left[\Delta n_\gamma \left(A_\pi^\Sigma(\Lambda\pi) + \frac{R_{\Lambda\pi}^{\Sigma\pi}}{2} A_\pi^\Sigma(\Sigma\pi)\right)\right. \\ &\left. -\Delta n_\pi \left(A_\gamma^\Sigma(\Lambda\pi) + \frac{R_{\Lambda\pi}^{\Sigma\pi}}{2} A_\gamma^\Sigma(\Sigma\pi)\right)\right), \end{aligned} \quad (6)$$

where terms starting with A are acceptance factors (given below) and

$$\begin{aligned} \Delta n_\pi &= n_\pi - N_\pi(\Lambda^* \to \Sigma^+\pi^-) - N_\pi(\Lambda^* \to \Sigma^0\pi^0) \\ &\quad -N_\pi(\Lambda^* \to \Sigma^0\gamma) - N_\pi(\Lambda^* \to \Lambda\gamma), \quad (7) \\ \Delta n_\gamma &= n_\gamma - N_\gamma(\Lambda^* \to \Sigma^+\pi^-) - N_\gamma(\Lambda^* \to \Sigma^0\pi^0) \\ &\quad -N_\gamma(\Lambda^* \to \Sigma^0\gamma) - N_\gamma(\Lambda^* \to \Lambda\gamma), \quad (8) \end{aligned}$$

with n_γ (n_π) equal to the yield of the kinematic fits, representing the measured number of photon (pion) candidates. In the notation used, lower case n represents some observed count while upper case N represents the acceptance corrected or derived quantities, where the π and γ subscripts indicate the kinematic fit hypothesis and the decay channel is shown in the parentheses (note that Λ^* denotes the $\Lambda(1405)$). These corrections are necessary to take into account due to the fact that the structure of the background underneath the $\Sigma(1385)$ is not zero, which could lead to over-counting of the $\Sigma(1385)$ contribution. For the detector acceptance, the notation has the pion (photon) hypothesis from decay of the $\Sigma(1385)$ given by A_π^Σ (A_γ^Σ) so that $A_\gamma^\Sigma(\Lambda\pi)$ denotes the relative leakage of the $\Sigma^{*0} \to \Lambda\pi$ decay channel into the $\Lambda\gamma$ extraction and $A_\pi^\Sigma(\Lambda\gamma)$ denotes the relative leakage of the $\Lambda\gamma$ decay channel into the $\Lambda\pi$ extraction.

Table II lists all decay channels taken into consideration and the value of the acceptance for the confidence level cuts $P_{\pi^0}^a(\chi^2) \leq 0.1\%$ followed by $P_\gamma^b(\chi^2) > 10\%$ for the γ-hypothesis and $P_\gamma^a(\chi^2) \leq 0.1\%$ followed by $P_{\pi^0}^b(\chi^2) > 10\%$ for the π^0-hypothesis. Using this form for corrections, an estimate of the number n_Λ for the $\Lambda(1405)$ in our event sample is required. The corrections for the γ channel are given by

$$N_\gamma(\Lambda^* \to \Lambda\gamma) = \frac{A_\gamma^\Lambda(\Lambda\gamma) BR(\Lambda^* \to \Lambda\gamma) n_\Lambda}{A_{\gamma\pi}^\Lambda(\Sigma^0\pi^0) + A_{\gamma\pi}^\Lambda(\Sigma^+\pi^-)}, \quad (9)$$

$$N_\gamma(\Lambda^* \to \Sigma^0\gamma) = \frac{A_\gamma^\Lambda(\Sigma^0\gamma) BR(\Lambda^* \to \Sigma^0\gamma) n_\Lambda}{A_{\gamma\pi}^\Lambda(\Sigma^0\pi^0) + A_{\gamma\pi}^\Lambda(\Sigma^+\pi^-)} \quad (10)$$

$$N_\gamma(\Lambda^* \to \Sigma^0\pi^0) = \frac{A_\gamma^\Lambda(\Sigma^0\pi^0) n_\Lambda}{A_{\gamma\pi}^\Lambda(\Sigma^0\pi^0) + A_{\gamma\pi}^\Lambda(\Sigma^+\pi^-)}, \quad (11)$$

$$N_\gamma(\Lambda^* \to \Sigma^+\pi^-) = \frac{A_\gamma^\Lambda(\Sigma^+\pi^-) n_\Lambda}{A_{\gamma\pi}^\Lambda(\Sigma^0\pi^0) + A_{\gamma\pi}^\Lambda(\Sigma^+\pi^-)} \quad (12)$$

where BR is the branching ratio for the decay shown, and likewise for the π^0 channel.

Isospin symmetry is assumed so that $BR(\Sigma^0\pi^0) = BR(\Sigma^+\pi^-) = BR(\Sigma^-\pi^+) \approx 1/3$ for the $\Lambda(1405)$ decay channels. The subscript "$\gamma\pi$" denotes the acceptance for events that do not satisfy the confidence level cuts for either hypotheses of the kinematic fit (*i.e.* it is likely to come from some background reaction). The value for $BR(\Lambda(1405) \to \Lambda\gamma)$ is taken from Ref. [30].

In order to find n_Λ one can look at the events for which neither the γ nor the π^0 hypothesis is satisfied. The value of n_Λ is difficult to determine due to the non-Breit-Wigner shape of the $\Lambda(1405)$ decay. A better approach is to use Monte Carlo to fill the background according to its internal decay kinematics and normalize it to the data such that the MC matches the data, thereby giving an estimate of n_Λ.

Figure 10 shows the MC simulations matching to the data, giving our estimate for the n_Λ. This can be used to correct all backgrounds except for the K^*.

The $\gamma p \to K^{*0}\Sigma^+$ reaction was investigated with MC simulation and compared with data. This background was determined to have a negligible effect on the final result, since there is no Λ in the final state. For the $\gamma p \to K^{*+}\Lambda$ reaction, few events survive all of the cuts. To include corrections for the few events that do survive, an estimate of the K^{*+} background must be established.

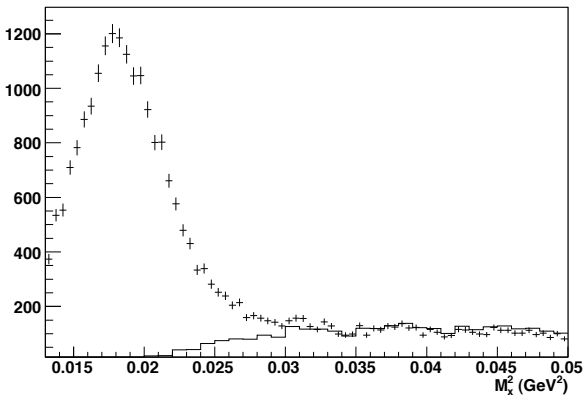

FIG. 10: Missing mass of $\gamma p \to K^+\Lambda(X)$ for data (points with error bars) and Monte Carlo simulations for the $\gamma p \to K^+\Lambda(1405)$ reaction (histogram) normalized to the data.

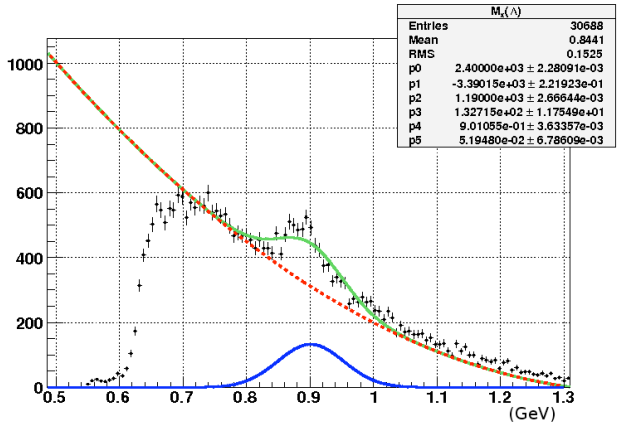

FIG. 11: Missing mass off the Λ fit with a Gaussian and with lower hyperon restrictions.

The correction for this background has the form

$$N_\pi(K^* \to K\pi^0) = \frac{n(K^{*+} \to K^+\pi^0)}{BR(K^{*+} \to K^+\pi^0)A_\pi(K^{*+} \to K^+\pi^0)}, \quad (13)$$

where $n(K^{*+} \to K^+\pi^0)$ is the estimated number of $K^{*+} \to K^+\pi^0$ events in our data sample. Assuming isospin symmetry, $BR(K^{*+} \to K^+\pi^0) = 1/3$ is the decay probability and $A_\pi(K^{*+} \to K^+\pi^0)$ is the acceptance under the π^0-hypothesis. Similarly, the radiative decay of the K^* has the form

$$N_\gamma(K^* \to K\gamma) = R(K^{*+} \to K^+\pi^0) \quad (14)$$
$$\times A_\pi(K^{*+} \to K^+\pi^0)N_\pi(K^* \to K\pi^0),$$

with $N_\pi(K^* \to K\pi^0)$ from the previous equation and $BR(K^{*+} \to K^+\gamma) \simeq 9.9 \times 10^{-4}$.

An estimate of the number of K^* events was obtained from matching the MC simulations to the data. The $K^{*+} \to K^+\pi^0$ mass distribution has been fit as shown in Fig. 11. In addition, fits to the $K^+\pi^0$ invariant mass were done by varying the kinematic cuts for the Σ^+ mass (see Fig. 3) to get more statistics, and the number of K^* events extrapolated to the nominal Σ^{*0} mass cut (1.34-1.43 GeV). Both methods gave similar results for $n(K^{*+} \to K^+\pi^0)$ used for the background correction in the final ratio.

Results

Following the above procedure for background subtraction, we now investigate the systematic uncertainties. Table III shows the final ratio, Eq. (6), for variations over a range of confidence level cuts. The primary source of variation is the secondary cut on P_γ.

The range of the systematic uncertainty in R in Table III is smaller than the statistical uncertainty, in part

TABLE III: Dependence of corrected branching ratio for variation of the confidence level cuts shown.

P_γ^b(%)	P_π^a(%)	R(%)
15	7.5	1.388± 0.12
15	5	1.390± 0.12
10	5	1.422± 0.12
10	1	1.420± 0.12
10	0.5	1.421± 0.12
5	0.1	1.448± 0.12
5	0.05	1.436± 0.12

because each combination of cuts has a large overlap of events (*i.e.* the same subset of events is present for all choices of cuts). Since the kinematic fit requires a constraint on the Λ mass, the kinematic cut on the invariant mass of the $p\pi^-$ has no effect. However, the other kinematic cuts (such as the Σ^{*0} mass cut) are unconstrained in the kinematic fit, and so these cuts were varied and their systematic uncertainties determined. In addition, the acceptances given in Table II are sensitive to the t-slope used to generate the MC simulations (which were tuned to fit the data) and so these systematic uncertainties were also determined. Adding each of the systematic uncertainty contributions in quadrature, upper and lower bounds in uncertainty were found for the ratio.

The final calculated ratio with all uncertainties is

$$R_{\Lambda\pi}^{\Lambda\gamma} = \frac{\Gamma[\Sigma^0(1385) \to \Lambda\gamma]}{\Gamma[\Sigma^0(1385) \to \Lambda\pi^0]} = 1.42 \pm 0.12(stat)^{+0.11}_{-0.07}(sys) \quad (15)$$

Previously published work [11] on this branching ratio yielded a ratio of $1.53 \pm 0.39^{+0.15}_{-0.17}$. The value given here is consistent within uncertainties of the previous value, but has smaller uncertainties. The smaller uncertainty is important, as the previous uncertainty was on the same order as the theoretical meson cloud corrections to the EM decay of the Δ. If similar meson cloud corrections

are to be proven true for EM decay of the Σ^{*0} baryon, then the smaller experimental uncertainty is a significant improvement.

In addition, the larger statistics of the current data set allow a better exploration of the systematic uncertainties. Although our systematic uncertainty is about the same as for the previously published ratio, the larger statistics allow for a more reliable determination of the systematic uncertainties.

The authors thank the staff of the Thomas Jefferson National Accelerator Facility who made this experiment possible. This work was supported in part by the bla bla bla...

[1] M.A.B. Bég, B.W. Lee and A. Pais, Phys. Rev. Lett. **13**, 514 (1964).
[2] H.R. Rubinstein, F. Scheck, and R.H. Socolow, Phys. Rev. **154**, 1608 (1967).
[3] N. Isgur and G. Karl, Phys. Rev. D **21**, 3175 (1980).
[4] C. Amsler *et al.* (Particle Data Group), Phys. Lett. B **667**, 1 (2008).
[5] J. Ashman *et al.*, Phys. Lett. B **206**, 364 (1988).
[6] S.J. Brodsky, J. Ellis, and M. Karliner, Phys. Lett. B **206**, 309 (1988).
[7] A. Deshpande, R. Milner, R. Venugopalan, and W. Vogelsong, Ann. Rev. Nucl. Part. Sci. **55**, 165 (2005).
[8] R.H. Dalitz and D.G. Sutherland, Phys. Rev. **146**, 1180 (1966).
[9] T. Sato and T.S.-H. Lee, Phys. Rev. C **54**, 2660 (1996).
[10] B. Juliá-Díaz, T.-S.H. Lee, T. Sato, and L.C. Smith, Phys. Rev. C **75**, 015205 (2007).
[11] S. Taylor *et al.* , Phys. Rev. C **71**, 054609 (2005); *ibid.* **72**, 039902 (2005).
[12] N. Isgur and G. Karl, Phys. Rev. D **20**, 1191 (1979).
[13] J. W. Darewych, M. Horbatsch, and R. Koniuk, Phys. Rev. D **28** 1125 (1983).
[14] R. Koniuk and N. Isgur, Phys. Rev. D **21**, 1868 (1980); Erratum: *ibid.* **23**, 818 (1981).
[15] M. Warns, W. Pfeil, and H. Rollnik, Phys. Lett. B **258**, 431 (1991).
[16] G. Wagner, A. J. Buchmann, and A. Faessler, Phys. Rev. C **58**, 1745 (1998).
[17] E. Kaxiras, E.J. Moniz, and M. Soyeur Phys. Rev. D **32**, 695 (1985).
[18] C. L. Schat, C. Gobbi, and N. B. Scoccola, Phys. Lett. B **356**, 1 (1995).
[19] A. Abada, H. Weigel, and H. Reinhardt, Phys. Lett. B **366**, 26 (1996).
[20] T. Haberichter, H. Reinhardt, N. N. Scoccola and H. Weigel, Nucl. Phys. A **615**, 291 (1997).
[21] R. Bijker, F. Iachello, and A. Leviatan, Annals Phys. **284**, 89 (2000).
[22] M. N. Butler, M. J. Savage, and R. P. Springer, Nucl. Phys. B **399**, 69 (1993).
[23] J. W. C. McNabb *et al.* , Phys. Rev. C **69** 042201 (2004).
[24] R. Bradford *et al.* , Phys. Rev. C **73** 035202 (2006).
[25] M. E. McCracken *et al.* , Phys. Rev. C **81** 025201 (2010).
[26] D. I. Sober *et al.* , Nucl. Instrum. Meth. A **440**, 263 (2000).
[27] B. A. Mecking *et al.* , Nucl. Instrum. Meth. A **503**, 513 (2003).
[28] D. Keller "Techniques in Kinematic Fitting", Jefferson Lab, CLAS-NOTE 2010-000.
[29] CERN-CN Division, GEANT 3.2.1, CERN Program Library W5013 (1993).
[30] H. Burkhardt and J. Lowe, Phys. Rev. C **44**, 607 (1991).